Heliyon 10 (2024) e28673

Contents lists available at ScienceDirect

Heliyon

journal homepage: www.cell.com/heliyon

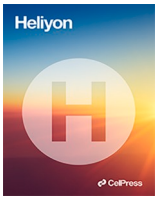

Research article

The prognostic model and immune landscape based on cancer-associated fibroblast features for patients with locally advanced rectal cancer

Huajun Cai [a,1], Yijuan Lin [b,1], Yong Wu [a,1], Ye Wang [a], Shoufeng Li [a], Yiyi Zhang [a], Jinfu Zhuang [a], Xing Liu [a], Guoxian Guan [a,c,*]

[a] *Department of Colorectal Surgery, The First Affiliated Hospital of Fujian Medical University, Fuzhou, China*
[b] *Department of Gastroenterology, The First Affiliated Hospital of Fujian Medical University, Fuzhou, China*
[c] *Department of Colorectal Surgery, National Regional Medical Center, Binhai Campus of The First Affiliated Hospital of Fujian Medical University, Fuzhou, China*

ARTICLE INFO

Keywords:
Cancer-associated fibroblasts
Locally advanced rectal cancer
Prognostic risk signature
Nomogram
Immune landscape

ABSTRACT

Background: This study aimed to construct a nomogram based on CAF features to predict the cancer-specific survival (CSS) rates of locally advanced rectal cancer (LARC) patients.
Methods: The EPIC algorithm was employed to calculate the proportion of CAFs. based on the differentially expressed genes between the high and low CAF proportion subgroups, prognostic genes were identified via LASSO and Cox regression analyses. They were then used to construct a prognostic risk signature. Moreover, the GSE39582 and GGSE38832 datasets were used for external validation. Lastly, the level of immune infiltration was evaluated using ssGSEA, ESTIMATE, CIBERSORTx, and TIMER.
Results: A higher level of CAF infiltration was associated with a worse prognosis. Additionally, the number of metastasized lymph nodes and distant metastases, as well as the level of immune infiltration were higher in the high CAF proportion subgroup. Five prognostic genes (SMOC2, TUBAL3, C2CD4A, MAP1B, BMP8A) were identified and subsequently incorporated into the prognostic risk signature to predict the 1-, 3-, and 5-year CSS rates in the training and validation sets. Differences in survival rates were also determined in the external validation cohort. Furthermore, independent prognostic factors, including TNM stage and risk score, were combined to established a nomogram. Notably, our results revealed that the proportions of macrophages and neutrophils and the levels of cytokines secreted by M2 macrophages were higher in the high-risk subgroup. Finally, the prognostic genes were significantly associated with the level of immune cell infiltration.
Conclusion: Herein, a nomogram based on CAF features was developed to predict the CSS rate of LARC patients. The risk model was capable of reflecting differences in the level of immune cell infiltration.

* Corresponding author.
E-mail address: fjxhggx@163.com (G. Guan).
[1] These authors contributed equally to this work.

https://doi.org/10.1016/j.heliyon.2024.e28673
Received 24 November 2023; Received in revised form 13 March 2024; Accepted 21 March 2024
Available online 26 March 2024

1. Introduction

As is well documented, colorectal cancer is one of the leading causes of death worldwide and is characterized by high morbidity and cancer-related mortality rates [1,2]. The majority of rectal cancer patients present with locally advanced disease at diagnosis and are recommended to undergo neoadjuvant chemoradiotherapy (NCRT). Despite locally advanced rectal cancer (LARC) patients benefiting from neoadjuvant treatment and surgical procedures [3–5], the long-term prognosis varies [6,7]. Accumulating evidence suggests that the close relationship between rectal tumor cells and cellular components of the tumor microenvironment (TME) in LARC patients influences survival outcomes [8–10]. Each cellular component in the TME (e.g., stromal and immune cells) exerts distinct functions (e.g., paracrine effects and immune response) and participates in tumor progression. Consequently, different proportions of cellular components in the TME among LARC patients undergoing NCRT can result in varying clinical outcomes [11]. Thus, it is pivotal to expand our understanding of the TME in those patients.

Cancer-associated fibroblasts (CAFs) are predominant stromal components of the tumor microenvironment [12,13]. Earlier studies have documented an intimate association between CAFs and the progression of numerous tumors, including LARC [14,15]. Via the secretion of multiple growth factors, cytokines, and chemokines, CAFs promote cancer cell proliferation and invasion, remodel the extracellular matrix, modulate immune responses, and confer resistance to treatment, thereby affecting prognosis [16–18]. However, studies on the prognostic role of CAFs in LARC patients are scarce. Besides, most bioinformatics studies have focused on the prognostic assessment of colon cancer rather than rectal cancer. Given the correlation between CAFs and the prognosis of cancers, there is an urgent need to identify CAF-related biomarkers to effectively predict prognoses and explore their potential mechanisms in LARC patients.

In the current study, the prognosis, clinicopathologic features, and TME status of the high CAF proportion subgroup were compared with the low CAF proportion subgroup in LARC patients. Next, a prognostic risk signature and nomogram were developed and validated based on the differentially expressed genes (DEGs) between the high and low CAF proportion subgroups. Finally, the immune cell infiltration status was explored in the high- and low-risk subgroups.

2. Method

2.1. Data acquisition

The GSE87211 [19] dataset, including the information on LARC patients undergoing NCRT, was initially downloaded. Afterward, raw data were extracted from the Gene Expression Omnibus database (GEO, http://www.ncbi.nlm.nih.gov/geo) and inputted into the R software. The backgroundCorrect function (method = normexp) of the "limma" package was utilized for background correction, while raw data were normalized via the normalizeBetweenArrays function [20]. Probes were annotated, and the annotated data were used in the subsequent analyses. Data on clinicopathological factors, including age, gender, pT stage, pN stage, pM stage, survival time, and survival status, were collected. Patients with missing data on age, tumor stage, and survival information were excluded from this study. The primary endpoint of this study was the cancer-specific survival (CSS) rate. A total of 195 patients were included in this study. The training and validation sets were randomly generated using the "caret" R package. This study was approved by the Ethics Committee of the First Affiliated Hospital of Fujian Medical University.

2.2. CAFs infiltration and TME assessment

Estimate the Proportion of Immune and Cancer cells (EPIC, https://epic.gfellerlab.org), based on a specific set of RNA-seq reference gene expression datasets, is an effective deconvolution tool for assessing the proportion of various cellular components within the TME [21]. In the GSE87211 dataset, the EPIC algorithm was used to determine to compute the abundance of CAFs in the TME of LARC patients. The EPIC score was calculated for each patient, and the high and low CAF proportion subgroups were defined based on the median of the proportion of CAFs.

The Estimation of STromal and Immune cells in MAlignant Tumor tissues using the Expression (ESTIMATE) algorithm was used to evaluate the levels of stromal cell and immune cell infiltration in the TME [22]. Thereafter, the "estimate" R package was used to execute the ESTIMATE algorithm on expression profiles to determine the stromal score, immune score, and estimate score. These scores were subsequently compared between the high and low CAF proportion subgroups to explore differences in cell infiltration.

2.3. Prognostic risk signature and nomogram

Differentially expressed genes (DEGs) between the high and low CAF proportion subgroups were identified according to the following criteria: absolute log2 (fold change) > 0.5 and the false discovery rate (FDR) < 0.05. Univariate Cox regression was employed to identify prognostic genes with a significance threshold of $P < 0.05$. Furthermore, independent prognostic genes were determined via least absolute shrinkage and selection operator (LASSO) regression using the "glmnet" R package and multivariate Cox survival analyses. Following this, the prognostic risk signature was constructed based on independent prognostic genes and their corresponding coefficient. The risk score was calculated using the following formula: risk score $= \beta_{\text{gene 1}} \times \text{Expression}_{\text{gene 1}} + \beta_{\text{gene 2}} \times \text{Expression}_{\text{gene 2}} + \beta_{\text{gene 3}} \times \text{Expression}_{\text{gene 3}} + \ldots + \beta_{\text{gene n}} \times \text{Expression}_{\text{gene n.}}$ In other words, a risk score was calculated for each case. Patients were assigned to either the high-risk subgroup or the low-risk subgroup based on the median risk score. Then, differences in clinical outcomes were analyzed between the two subgroups. Moreover, the area under the receiver-operating characteristic (AUROC)

curve was calculated to evaluate the accuracy of the prognostic risk signature. Of note, higher AUC values correspond to superior predictive values. A nomogram was generated based on independent prognostic factors using the R package "rms". Individualized 1-, 3-, and 5-year CSS rates were predicted using this model. The performance of the nomogram was evaluated using the Harrell's concordance index (C-index), and the calibration curve was applied to assess the accuracy of the model-predicted survival compared to actual 1-, 3-, and 5-year CSS rates.

2.4. Validation datasets

Regarding the validation of the prognostic risk signature, external validation cohorts were collected from the GEO database. The GSE39582 dataset comprised a total of 585 samples, excluding 19 non-tumoral samples and 9 patients with unknown relapse-free survival (RFS) information. Finally, 557 patients were included in the analysis. Additionally, 122 patients with colorectal cancer from the GSE38832 dataset were also included.

2.5. Functional enrichment analysis

Regarding the assessment of differences in potential biological mechanisms between the high- and low-risk subgroups, gene set enrichment analysis (GSEA) was performed using hallmark gene sets (v7.2) from the Molecular Signatures Database (MSigDB, https://software.broadinstitute.org/gsea/msigdb/) [23]. An FDR q-value <0.25 was considered statistically significant.

2.6. Immune landscape

The correlation between risk scores and biomarkers of CAFs was initially determined. Given that CAFs interact with other immune cells in a paracrine manner, the relationship between risk scores and CAF-secreted cytokines was investigated. To further examine the level of immune cell infiltration between the two subgroups, single sample gene set enrichment analysis (ssGSEA) was conducted using the R package "gsva" [24]. Then, the enrichment scores of various immune cell components were determined, reflecting the relative abundances of immune cells in TME. The correlation between gene expression and immune cells was assessed using Tumor Immune Estimation Resource (TIMER) [25].

Moreover, Cell-type Identification By Estimating Relative Subsets of RNA Transcripts (CIBERSORTx, https://cibersortx.stanford.edu/) was used to evaluate the immune status [26]. The relationship between risk score and macrophage subtypes (M0, M1, and M2) was also assessed. Lastly, the levels of cytokines secreted by M2 macrophages across different risk scores were determined [27,28].

2.7. Statistical analysis

Statistical analyses were performed using R software (version 3.6.3) and GraphPad Prism 8. Between-group differences were assessed using the Wilcoxon Rank-sum test. The "pheatmap" R package was employed for generating heatmaps. Survival analysis and Kaplan-Meier (KM) curves were performed using the R package "survival". Principal component analysis (PCA) and t-distributed Stochastic Neighbor Embedding (tSNE) were performed for dimension reduction, followed by data visualization using the R package "ggplot2". The Spearman correlation test was used for correlation analysis. $P < 0.05$ is deemed statistically significant.

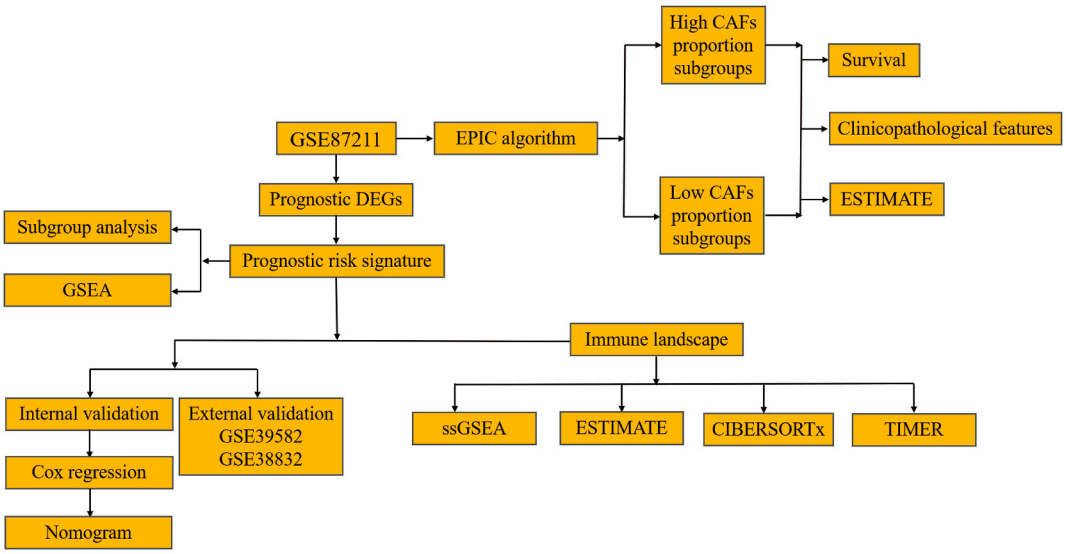

Fig. 1. Study flow diagram.

3. Results

3.1. CAF proportions in LARC patients

The flow diagram of this study is depicted in Fig. 1. Based on the median of CAF proportion acquired from the EPIC algorithm, 92 and 103 patients were included in the high and low CAF proportion subgroups, respectively. Their clinicopathologic features are listed in Supplementary Table 1. A significant difference was observed in CSS between the two subgroups, with patients with high CAF infiltration exhibiting worse clinical outcomes (Fig. 2A). Next, the relationship between clinicopathologic features and CAF proportion was evaluated (Fig. 2B–F). The analysis exposed that high CAF proportion was significantly associated with lymph node metastasis and distant metastasis (all $P < 0.05$), whereas age, gender, and pT stage were comparable between the two subgroups. Considering the close intracellular communication between CAFs and cellular components, differences in stromal and immune cell infiltration were further compared between the subgroups. As anticipated, the ESTIMATE score, stromal score, and immune score of the high CAF proportion subgroup were significantly higher than those of the low CAF proportion subgroup (Fig. 2G–I). These results collectively indicated that CAFs promote LARC progression and affect survival and that the prognostic risk signature based on CAF-related characteristics holds potential for clinical application.

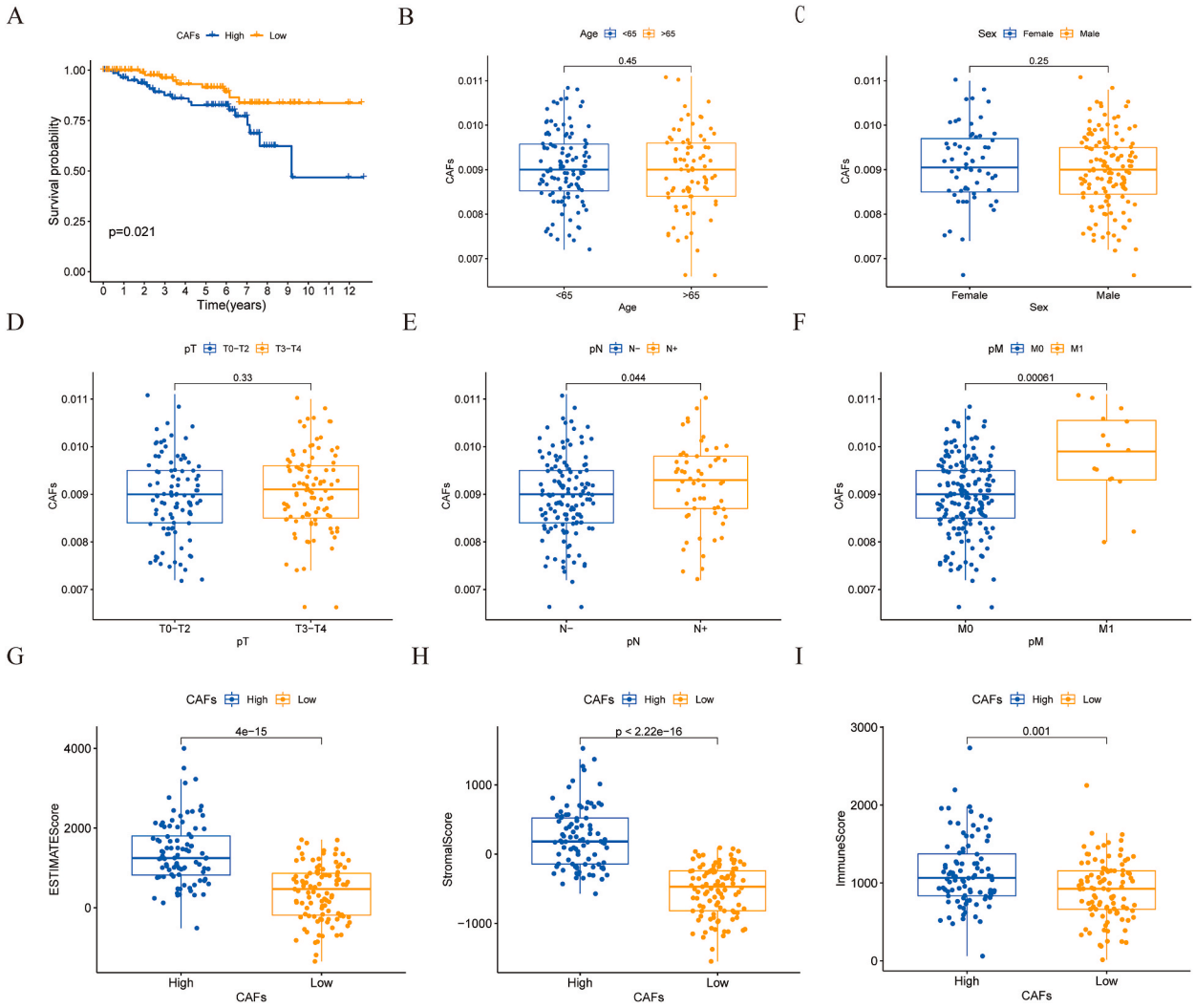

Fig. 2. Kaplan–Meier survival curves depicting the prognostic value of CAFs in LARC patients undergoing NCRT (A), differences in clinicopathological features and immune infiltration levels between the high and low CAF proportion subgroups: age (B), gender (C), pT stage (D), pN stage (E), pM stage (F), ESTIMATE score (G), stromal score (H), immune score (I). CAF: cancer-associated fibroblasts; LARC: locally advanced rectal cancer; NCRT: neoadjuvant chemoradiotherapy.

3.2. Development and validation of the prognostic risk signature

1022 DEGs were identified between the high and low CAF proportion subgroups. Then, patients were randomized into a training set and a validation set (Table 1). In the training set, 19 genes were found to be positively correlated with prognosis. Meanwhile, LASSO regression (Fig. 3A–B) and multivariate Cox regression (Fig. 3C) analyses yielded 5 independent prognostic genes (SMOC2, TUBAL3, C2CD4A, MAP1B, and BMP8A). Next, the prognostic risk signature was constructed based on the expression levels of independent prognostic genes and their corresponding coefficient: 0.633 × SMOC2+1.030 × TUBAL3—0.952 × C2CD4A+1.252 × MAP1B+1.252 × BMP8A. Afterward, the risk score was calculated for each individual. Patients were further stratified into high- and low-risk subgroups based on the median risk score for the ensuing analyses. In addition, the expression levels of independent prognostic genes in the training and validation sets were detected. As illustrated in Fig. 3D–E, the expression level of SMOC2, TUBAL3, MAP1B, and BMP8A was higher in the two sets, whereas that of CD4A was low. At the same time, survival analyses determined that higher scores were significantly correlated with worse clinical outcomes in the training set (Fig. 4A–B), consistent with the findings in the validation set (Fig. 4D–E). Interestingly, the AUC values for the 1-, 3-, and 5-year CSS rates were 0.864, 0.946, and 0.947 in the training set (Fig. 4C), 0.716 and 0.696, 0.701 in the validation set, respectively (Fig. 4F). Finally, the ROC curves displayed that the prognostic risk signature had satisfactory predictive strength in both sets.

3.3. Construction of the nomogram

There was a significant difference in survival rates between the high- and low-risk subgroups in the whole set ($P < 0.001$, Fig. 5A). As is well documented, the combination of independent prognostic factors further enhances predictive abilities. Consequently, univariate and multivariate Cox analyses were performed to identify independent prognostic factors. As delineated in Fig. 5B–C, TN and risk scores were significantly and independently correlated with CSS. The nomogram was subsequently constructed by incorporating significant variables to predict the 1-, 3-, and 5-year CSS rates for LARC patients undergoing NCRT (Fig. 5D). The nomogram demonstrated accurate prognostic accuracy, with a C-index of 0.827 (95% confidence interval: 0.745–0.909). Besides, the calibration curves exhibited excellent agreement between the predictive- and actual 1-, 3-, and 5-year CSS rates (Fig. 5E).

3.4. External validation of the prognostic risk signature

Based on the gene expression of the signature, the risk score was calculated in the external validation cohort. As illustrated in Fig. 6A, the difference in RFS was significant, with the high-risk group exhibiting worse clinical outcomes ($P = 0.024$) in the GSE39582 cohort. Likewise, the high-risk group was also linked to shorter CSS rates in the GSE38832 cohort ($P = 0.024$, Fig. 6B). Furthermore, the ROC curves (Fig. 6C–5D) indicated that the risk score could efficiently predict survival in both cohorts (GSE39582: AUC = 0.576, $P = 0.004$; GSE38832: AUC = 0.698, $P = 0.002$).

Table 1
Clinicopathological features of patients in training set and validation set.

Characteristics	Training set	Validation set
	N (%)	N (%)
Age, years		
<65	58(59.2)	56(57.7)
>65	40(40.8)	41(42.3)
Sex		
Female	32(32.7)	28(28.9)
Male	66(67.3)	69(71.1)
pT stage		
T0	18(18.4)	15(15.5)
T1	10(10.2)	11(11.3)
T2	20(20.4)	23(23.7)
T3	43(43.9)	44(45.4)
T4	7(7.1)	4(4.1)
pN stage		
N0	66(67.3)	72(74.2)
N1	24(24.5)	18(18.6)
N2	8(8.2)	7(7.2)
pM stage		
M0	90(91.8)	90(92.8)
M1	8(8.2)	7(7.2)
TNM stage		
pCR	18(18.4)	15(15.5)
Stage I	23(23.5)	30(30.9)
Stage II	21(21.4)	26(26.8)
Stage III	28(28.6)	19(19.6)
Stage IV	8(8.2)	7(7.2)

TNM: tumor-node-metastasis, pCR: pathologic complete response.

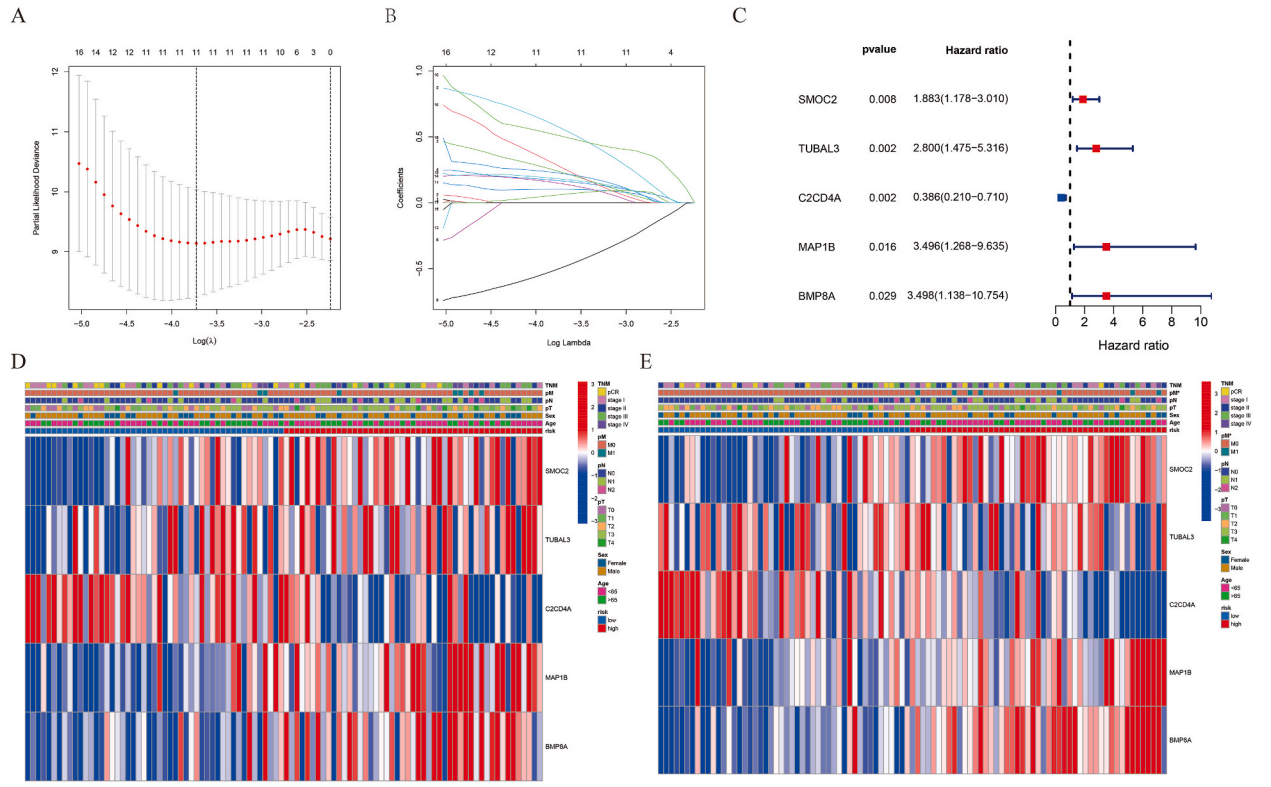

Fig. 3. Identification of independent prognostic CAF-related genes by LASSO regression (A–B) and multivariable Cox regression (C) in the training set. Differential expression of five CAF-related genes in the training set (D) and validation set (E). CAF: cancer-associated fibroblasts; LASSO: least absolute shrinkage and selection operator.

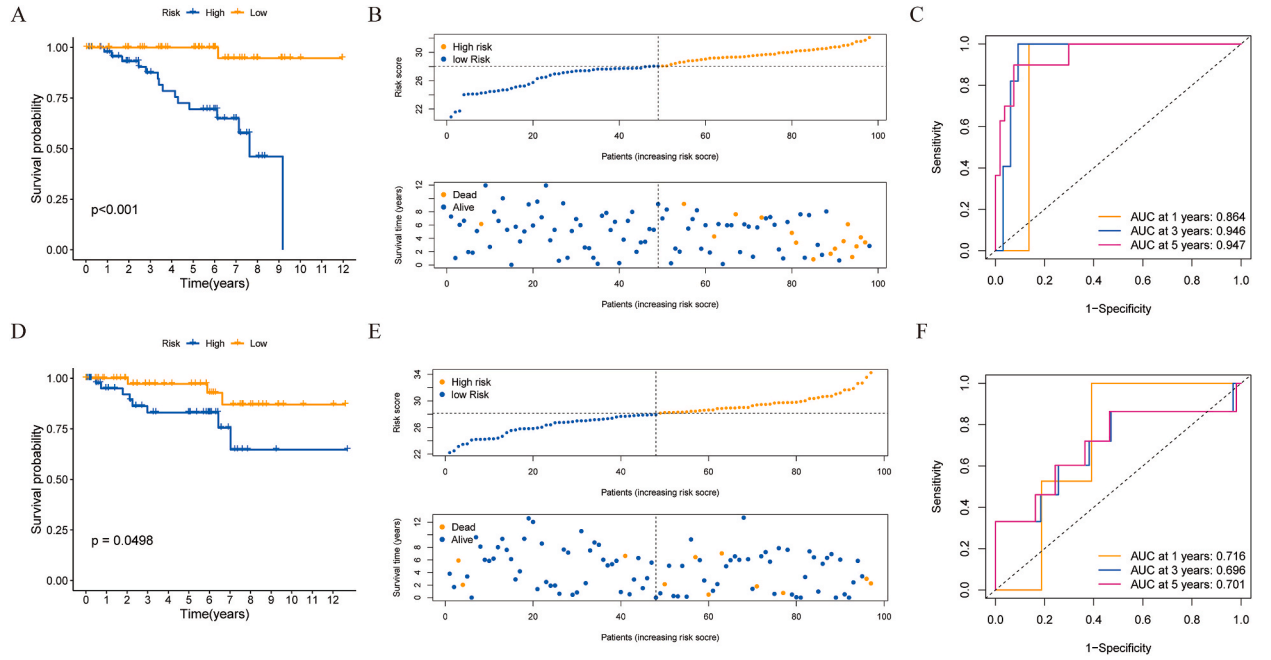

Fig. 4. The predictive capability of the prognostic risk signature. Kaplan–Meier survival curves between the high- and low-risk subgroups in the training set (A) and validation set (D), the risk score distribution plot in the training set and (B) validation set (E), ROC curve for predicting 1-, 3-, and 5-year CSS rates in training the set and (C) validation set (F). ROC: receiver-operating characteristic, CSS: cancer-specific survival.

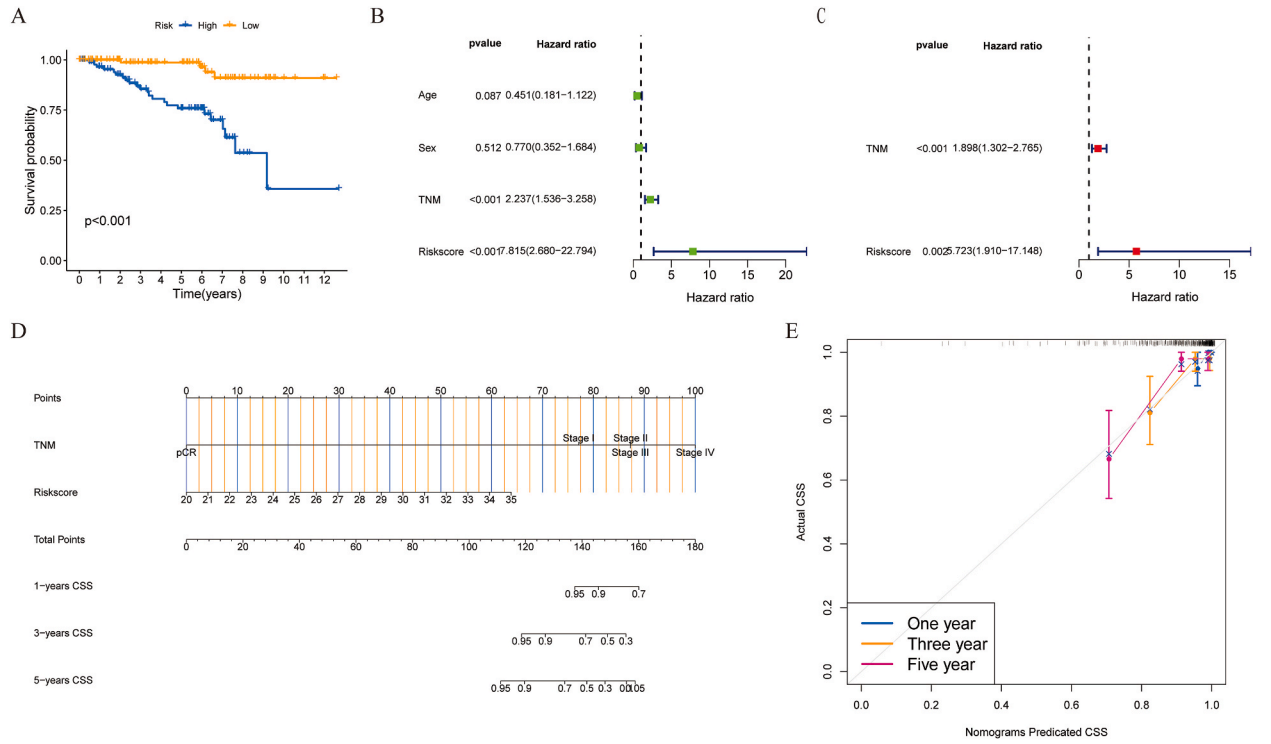

Fig. 5. The construction of the nomogram to predict CSS rates for LARC patients undergoing NCRT. Kaplan–Meier survival curves between the high- and low-risk subgroups (A), identification of independent prognostic factors via univariate (B) and multivariate Cox analyses (C), development of nomogram to predict CSS rates (D), and model assessment via the calibration curve (E). CSS: cancer-specific survival, LARC: locally advanced rectal cancer; NCRT: neoadjuvant chemoradiotherapy.

3.5. Subgroup analysis of clinicopathologic features

To further validate the predictive capability of the prognostic risk signature, subgroup analyses were performed on clinicopathologic features such as age, gender, pT stage, pN stage, and pM stage (Fig. 7A–J). The analysis uncovered significant differences between the high- and low-risk subgroups in patients aged <65 years, gender, pT3-4 stage, pN stage, and pM0 stage (all $P < 0.05$), demonstrating the outstanding predictive value of the risk signature.

3.6. Visualization and potential mechanism of high- and low-risk subgroup

The benefits of the prognostic risk signature were further supported by the PCA and tSNE plots. As displayed in Fig. 8A–B, the risk subgroups were clearly discriminated. Furthermore, GSEA was performed to discover potential biological pathways in the high- and low-risk subgroups. Noteworthily, the high-risk subgroup was enriched in pathways related to angiogenesis, epithelial-mesenchymal transition (EMT), hypoxia, inflammatory response, apoptosis, complement, Notch signaling, Wnt/β-catenin signaling, and TGF-βsignaling pathway (Fig. 8C). These results can contribute to a better understanding of malignant biological behaviors and warrant further investigation.

3.7. Analysis of immune infiltration

The expression of CAF-related biomarkers was detected across different risk scores. A significant correlation was observed between the risk score and CAF-associated biomarkers (e.g., ACTA2, FAP, FSP1, S100A4) (Fig. 9A), implying the prognostic risk signature was characterized by CAFs and that CAFs exert biological functions through the secretion of cytokines. Consequently, the correlation between risk scores and cytokines secreted by CAFs was further investigated. The correlation heatmap (Fig. 9B) validated that the levels of cytokines (e.g., IL-6, CXCL-12, FGF2, CCL2) were higher in the high-risk subgroup.

As portrayed in Fig. 9C–D, the stromal scores and immune scores were significantly higher in the high-risk subgroup. CAFs have been reported to interact with other cellular components in the TME and synergistically influence tumor progression. Hence, the level of immune infiltration in the two risk subgroups was investigated by conducting ssGSEA. The results unveiled that the number of macrophages was higher in the high-risk subgroup (Fig. 9E–F). Macrophages typically display two polarization states, namely activated macrophages (M1) and alternatively activated macrophages (M2). Thus, the CIBERSORTx algorithm was adopted to explore

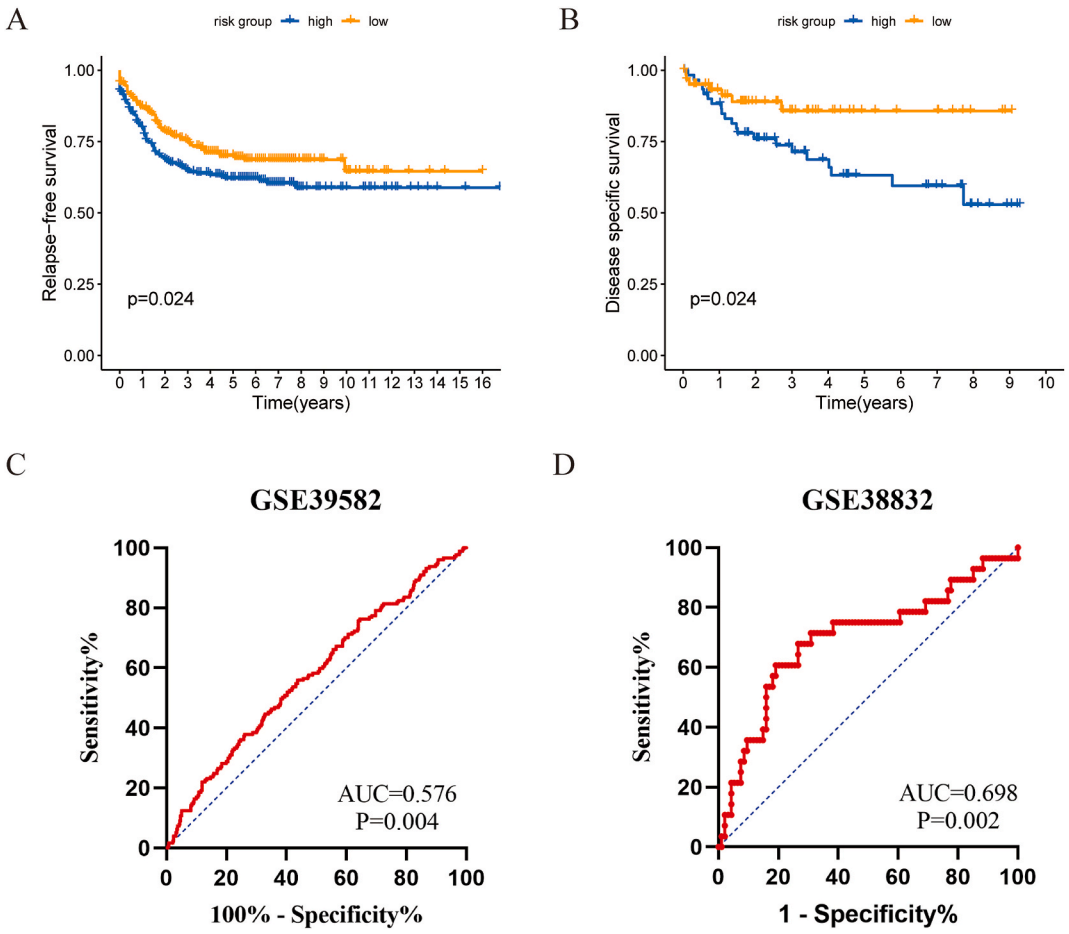

Fig. 6. External validation of the prognostic risk signature. Kaplan–Meier survival curves between the high- and low-risk subgroups in the GSE39582 (A) and GSE38832 datasets (B) and the receiver-operating characteristic curves based on risk scores to predict survival rates in the GSE39582 (C) and GSE38832 datasets (D).

differences in the expression of M0 (unpolarized), M1, and M2 macrophages. A positive correlation was noted between risk score and M0 and M2 macrophages, which are pro-tumorigenic subtypes (Fig. 9G and I). In contrast, no significant differences were detected in M1 macrophages, the anti-tumor subtype (Fig. 9H). M2 macrophages release cytokines that participate in tumor proliferation and TME remodeling, and as shown in Fig. 9J, M2 macrophages released high levels of cytokines (e.g., CCL2, CCL14, IL-4, TGFβ-1) in the high-risk subgroup. Conversely, a higher degree of natural killer (NK) cell infiltration was detected in the low-risk subgroup. Similarly, the infiltration levels of B cells, neutrophils, and regulatory T (T-reg) cells were markedly different between the two subgroups (Fig. 9E–F).

In addition, correlations between the expression levels of the five prognostic genes and immune cells were determined using the TIMER database (Fig. 10A–E). The results revealed a positive correlation between BMP8A and B cells ($P = 0.009$), $CD4^+$ T cells ($P < 0.001$), macrophages ($P = 0.003$), neutrophils ($P = 0.024$), and dendritic cells ($P < 0.001$).

4. Discussion

At present, NCRT followed by total mesorectal excision is the gold standard for the treatment of LARC, demonstrating superiority in shrinking tumor size and stage, preserving the anal sphincter, and improving local tumor control [3,4]. This approach yields a pathologic complete response rate of approximately 10%–20% [29–31]. However, some LARC patients are unresponsive to NCRT due to differential treatment responses, which can result in varying survival outcomes [32]. More importantly, survival rates among patients with similar clinicopathologic features differed as well. Thus, pioneering an individualized prognostic model is warranted for LARC patients undergoing NCRT. In recent years, mounting evidence indicated that TME plays a crucial role in tumor progression and survival. As a principal cellular component in the TME, CAFs display a high degree of aggressive behaviors and enhanced secretory functions [33]. According to recent studies, CAFs confer treatment resistance by secreting cytokines and the delivery of exosomal vesicles in colorectal cancer [34–37]. Saigusa et al. reported that the up-regulated expression of biomarkers of CAFs, encompassing fibroblast activation protein-α (FAP-α) and stromal cell-derived factor-1, was correlated with a poor prognosis in LARC patients undergoing NCRT [8]. Furthermore, previous studies also identified FAP as a poor predictive factor in colorectal cancer [38]. It is evident

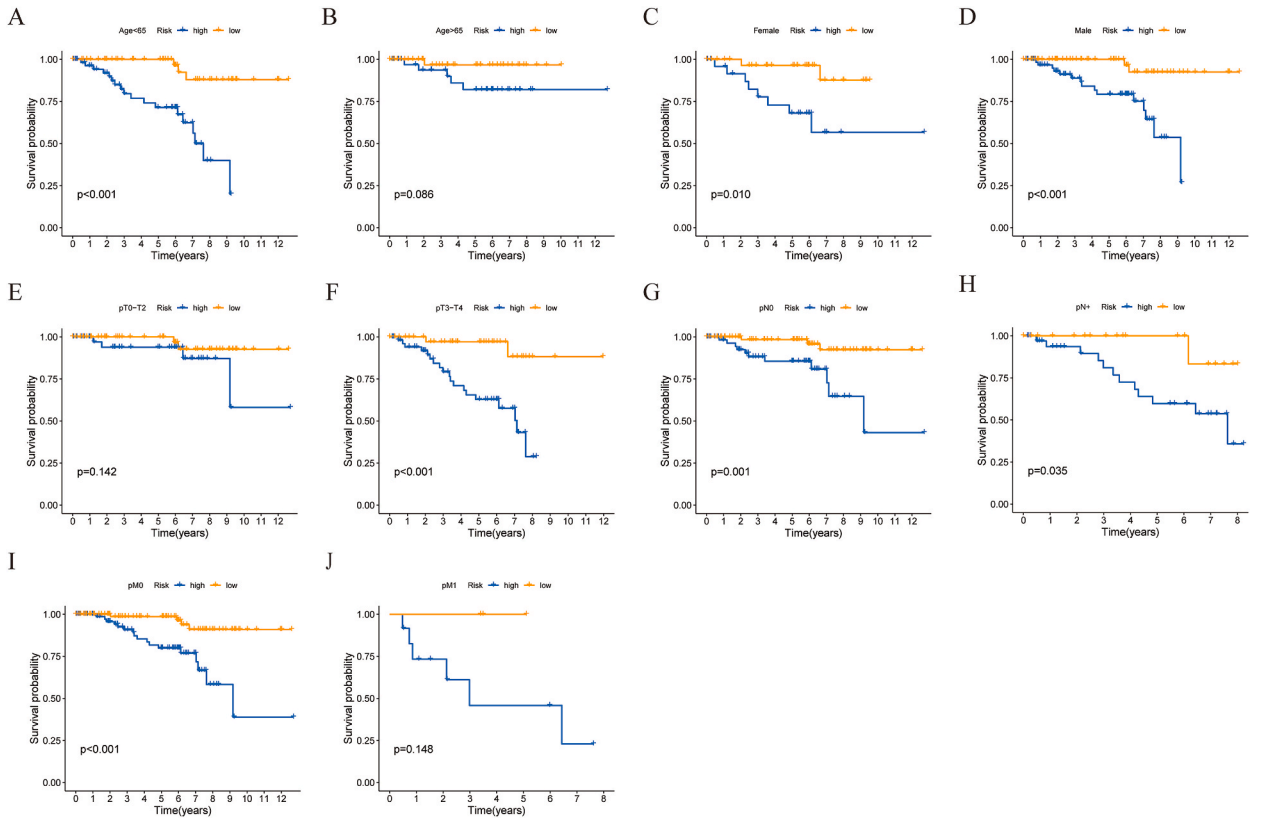

Fig. 7. Subgroup analysis according to clinicopathological features. Differences in survival rates between the high- and low-risk subgroups in patients aged <65 years (A), aged >65 years (B), female (C), male (D), pT0-T2 stage (E), pT3-T4 stage (F), pN0 stage (G), pN + stage (H), pM0 stage (I), pM1 stage (J). pCR: pathologic complete response, TNM: tumor-node-metastasis.

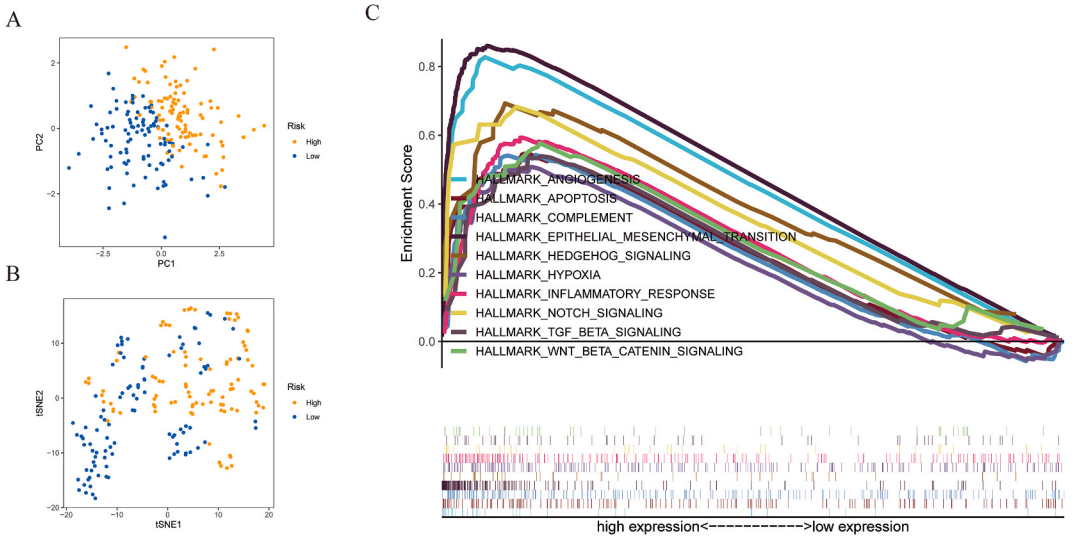

Fig. 8. The ability of the prognostic risk signature to distinguish between the high- and low-risk subgroups. PCA plot (A), tSNE plot (B), and GSEA for the high-risk subgroup (C). PCA: principal component analysis, tSNE: t-distributed Stochastic Neighbor Embedding, GSEA: gene set enrichment analysis.

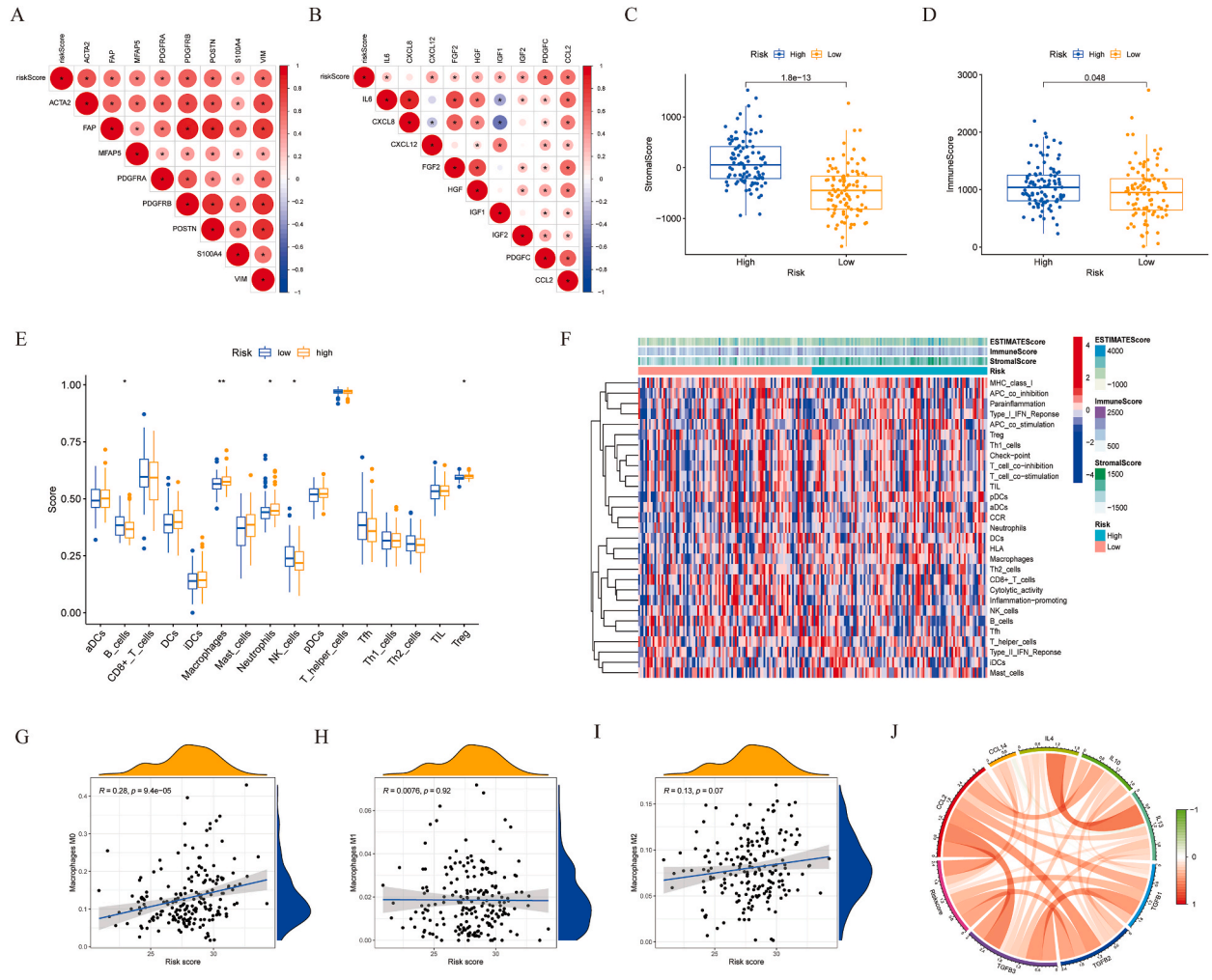

Fig. 9. Features of the prognostic risk signature and immune landscape. The correlation between risk scores and CAF-related biomarkers (A) and cytokines (B), the difference in stromal scores (C), immune scores (D), and infiltration of immune cells (E–F) between the high- and low-risk subgroups, The correlation between risk scores and macrophage subtypes (M0, M1, M2, G-I), The correlation between risk scores and cytokine related to M2 macrophages (J). CAF: cancer-associated fibroblasts, *: $P < 0.05$, **: $P < 0.01$.

that CAF infiltration is correlated with a poor prognosis in colorectal cancer patients. However, to the best of our knowledge, studies focusing on prognostic risk signatures based on CAF-related features for LARC patients undergoing NCRT are limited.

Herein, the level of CAF infiltration was calculated in LARC patients undergoing NCRT using the EPIC algorithm. Significant differences in survival rates were observed between the two subgroups, with the clinical outcomes of patients with a high level of CAF infiltration being worse. Noteworthily, lymph node metastases and distant metastases were more prevalent in the high CAF proportion subgroup, and the degree of immune cell and stromal cell infiltration was higher. Taken together, these findings demonstrate that CAFs impact the progression and prognosis of LARC patients undergoing NCRT, with the immunologic microenvironment potentially playing a synergistic role. Thus, we postulate that the CAF-related prognostic signature holds considerable application potential. Moreover, in the training set, independent prognostic-related genes (SMOC2, TUBAL3, C2CD4A, MAP1B, and BMP8A) were screened and identified from DEGs between the high and low CAF proportion subgroups. Following this, an individualized prognostic risk signature was constructed based on the expression of prognostic genes and their corresponding coefficients. Notably, this signature was accurate in predicting the 1-, 3-, and 5-year CSS rates in both the training and validation sets. Furthermore, a nomogram was constructed by combining the signature with independent prognostic factors in order to predict survival. This nomogram may contribute to the development of personalized treatment strategies and cancer surveillance. The pro-tumorigenic functions of C2CD4A are well documented [39]. Nevertheless, the role of SMOC2 in the progression of rectal cancer remains controversial [40,41]. Furthermore, the biological functions of TUBAL3, MAP1B, and BMP8A in rectal cancer remain to be elucidated.

In addition, the potential mechanism was also explored in the risk subgroups via GSEA analysis, which determined that the high-risk subgroup was significantly enriched in cancer-associated pathways, such as angiogenesis, EMT, hypoxia, inflammatory response, apoptosis, and TGF-βsignaling pathway. A recent study undertaken by Unterleuthner et al. evinced that CAFs secrete WNT2 that

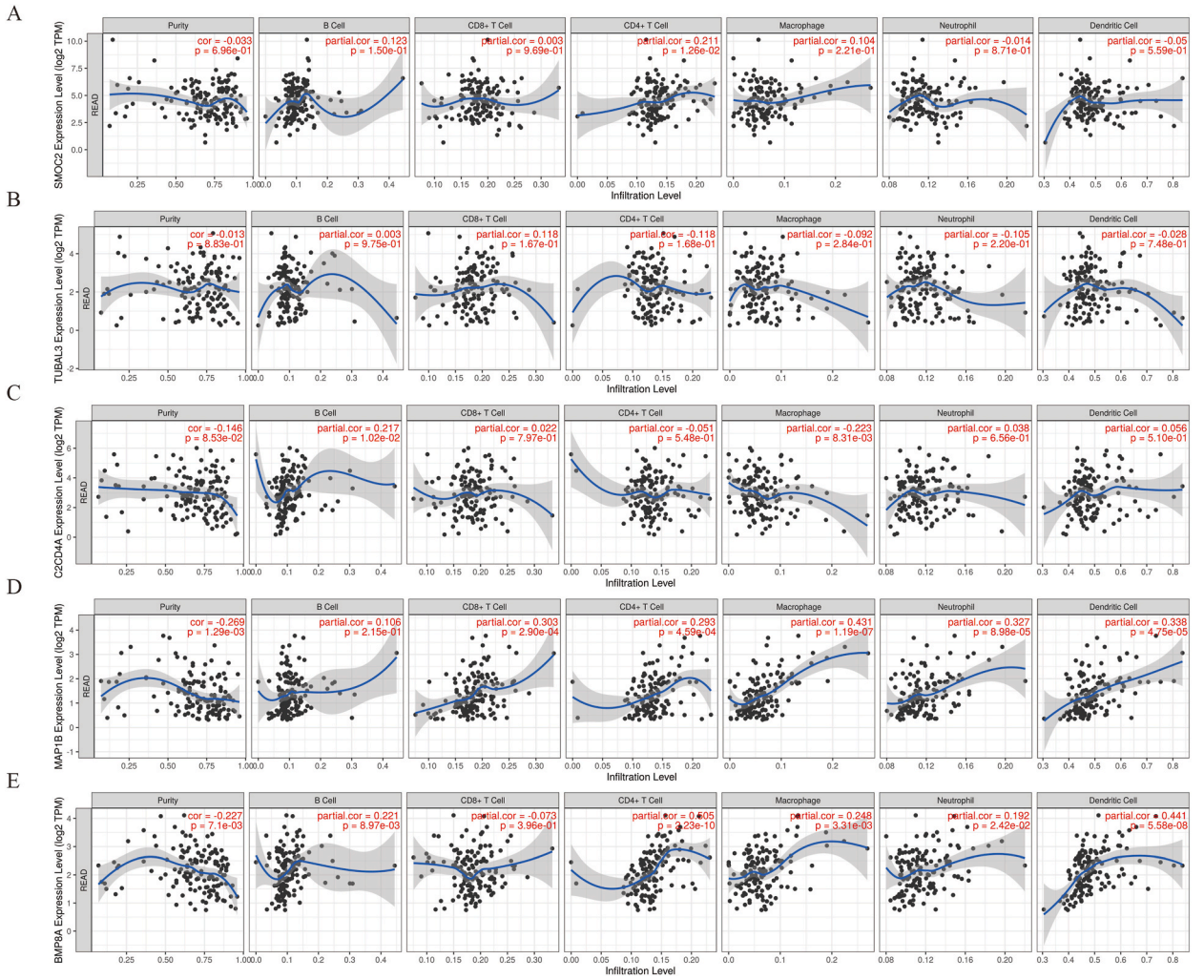

Fig. 10. The correlation between the expression level of SMOC2 (A), TUBAL3 (B), C2CD4A (C), MAP1B (D), and BMP8A (E) and immune cells (including B cells, $CD8^+$ T cells, $CD4^+$ T cells, macrophages, neutrophils, and dendritic cells).

promotes tumor angiogenesis in colon cancer [42]. One study indicated that CAFs promote the EMT of colorectal cancer cells by exosome-mediated intercellular communication [34]. Similar biologic behavior has also been described in gastric cancer [43], prostate cancer [44], and oral cancer [45]. Besides, the hypoxic microenvironment enhances the activity of CAFs, which in turn promotes tumor progression [46–48]. Exosomes derived from CAFs enhanced colorectal cancer cell stemness and promoted resistance to radiotherapy by activating the TGF-βpathway [37]. These results conjointly suggested the potential mechanisms in the high-risk subgroup.

It is worthwhile emphasizing that the level of macrophage infiltration was significantly different between the high- and low-risk subgroups. Specifically, the degree of M2 macrophage recruitment was higher in the high-risk subgroup. Indeed, macrophages constitute tumor-infiltrating immune cell components in the TME and exhibit two polarization states, namely classically activated M1 subtype and alternatively activated M2 subtype [49]. The former possesses a tumoricidal activity phenotype, whereas the latter stimulates tumor progression. The crosstalk between CAFs and macrophages has been described in recent studies. In colorectal cancer, the expression of biomarkers of M2 macrophages (CD206, CD163) has been reported to be up-regulated following co-culture with CAFs and macrophages [50]. In addition, macrophage colony-stimulating factor was secreted by CAFs to shift macrophages to the M2 polarization state and promote pancreatic ductal adenocarcinoma cell proliferation, migration, and invasion [51]. CAFs promote tumor metastasis and angiogenesis in prostate carcinoma in conjunction with M2 macrophages [52]. Moreover, the killing capacity of NK cells was inhibited after the synergistic interaction between CAFs and macrophages, protecting colorectal tumor cells against NK cells [50]. In melanoma, CAFs induce a decrease in the killing capacity of NK cells [53]. On the other hand, CAFs were found to be implicated in the regulation of T-reg cells, and a high level of T-reg cells was associated with a poor prognosis in lung adenocarcinoma [54]. Overall, these findings highlight that CAFs closely interact with immune cells to synergistically affect tumor characteristics, warranting further investigation into their role in colorectal cancer.

Nonetheless, some limitations of this study merit acknowledgment. To begin, the biological function of the five CAF-related genes

necessitates further exploration. Secondly, the detailed mechanism underlying intercellular communications between CAFs and immune cells requires further studies.

5. Conclusion

A higher CAF proportion was correlated with worse survival in LARC patients undergoing NCRT. Herein, a prognosis risk signature was established based on DEGs between the high and low CAF proportion subgroup. Furthermore, a nomogram was developed to predict the 1-, 3-, and 5-year CSS rates by incorporating independent prognostic factors into the model. Lastly, the risk model was also capable of reflecting differences in the level of immune cell infiltration.

Funding

This study was supported by National Natural Science Foundation of China (No. 82172800), Special Financial Foundation of Fujian Provincial (No. 2020B019), Joint Funds for the Innovation of Science and Technology, Fujian Province (No. 2020Y9125), Talent programs granted from The First Affiliated Hospital of Fujian Medical University (YJRC3600), and Startup Fund for Scientific Research of Fujian Medical University (No.2020QH2036).

Ethics statement

This study was reviewed and approved by the Ethics Committee of the First Affiliated Hospital of Fujian Medical University, with the approval number:2021323.

Data availability statement

Data is available from the GEO database (https://www.ncbi.nlm.nih.gov/geo, GSE87211, GSE39582, and GSE38832).

CRediT authorship contribution statement

Huajun Cai: Writing – original draft, Methodology, Funding acquisition, Formal analysis, Data curation, Conceptualization. **Yijuan Lin:** Methodology, Investigation. **Yong Wu:** Validation, Software. **Ye Wang:** Supervision. **Shoufeng Li:** Data curation. **Yiyi Zhang:** Methodology. **Jinfu Zhuang:** Supervision. **Xing Liu:** Supervision. **Guoxian Guan:** Writing – review & editing, Methodology, Funding acquisition, Conceptualization.

Declaration of competing interest

The authors declare that they have no known competing financial interests or personal relationships that could have appeared to influence the work reported in this paper.

Acknowledgments

All authors appreciate the GEO datasets platforms and contributors for their valuable datasets.

Appendix A. Supplementary data

Supplementary data to this article can be found online at https://doi.org/10.1016/j.heliyon.2024.e28673.

Abbreviations

LARC	locally advanced rectal cancer
CAFs	cancer-associated fibroblasts
CSS	cancer-specific survival
EPIC	Estimate the Proportion of Immune and Cancer cells
LASSO	least absolute shrinkage and selection operator
ssGSEA	single sample gene set enrichment analysis
ESTIMATE	Estimation of Stromal and Immune cells in Malignant Tumor tissues using Expression
CIBERSORTx	Cell-type Identification by Estimating Relative Subsets of RNA Transcripts
TIMER	Tumor Immune Estimation Resource
TNM	Tumor-node-metastasis
NCRT	neoadjuvant chemoradiotherapy
TME	tumor microenvironment
DEGs	differentially expressed genes

GEO	Gene Expression Omnibus
FDR	false discovery rate
AUC	area under the curve
ROC	receiver-operating characteristic
C-index	concordance index
RFS	relapse-free survival
PCA	principal component analysis
tSNE	t-distributed Stochastic Neighbor Embedding
T-reg	regulatory T
NK	natural killer
FAP-α	fibroblast activation protein-α

References

[1] H. Sung, J. Ferlay, R.L. Siegel, M. Laversanne, I. Soerjomataram, A. Jemal, F. Bray, Global cancer statistics 2020: GLOBOCAN estimates of incidence and mortality worldwide for 36 cancers in 185 countries, Ca - Cancer J. Clin. 71 (2021) 209–249. https://10.3322/caac.21660.

[2] R.L. Siegel, K.D. Miller, A. Goding Sauer, S.A. Fedewa, L.F. Butterly, J.C. Anderson, A. Cercek, R.A. Smith, A. Jemal, Colorectal cancer statistics, Ca - Cancer J. Clin. 70 (2020) (2020) 145–164. https://10.3322/caac.21601.

[3] W. van Gijn, C.A. Marijnen, I.D. Nagtegaal, E.M. Kranenbarg, H. Putter, T. Wiggers, H.J. Rutten, L. Påhlman, B. Glimelius, C.J. van de Velde, Preoperative radiotherapy combined with total mesorectal excision for resectable rectal cancer: 12-year follow-up of the multicentre, randomised controlled TME trial, Lancet Oncol. 12 (2011) 575–582. https://10.1016/s1470-2045(11)70097-3.

[4] M.S. Roh, L.H. Colangelo, M.J. O'Connell, G. Yothers, M. Deutsch, C.J. Allegra, M.S. Kahlenberg, L. Baez-Diaz, C.S. Ursiny, N.J. Petrelli, N. Wolmark, Preoperative multimodality therapy improves disease-free survival in patients with carcinoma of the rectum: nsabp R-03, J. Clin. Oncol. 27 (2009) 5124–5130. https://10.1200/jco.2009.22.0467.

[5] J. Kitz, E. Fokas, T. Beissbarth, P. Ströbel, C. Wittekind, A. Hartmann, J. Rüschoff, T. Papadopoulos, E. Rösler, P. Ortloff-Kittredge, U. Kania, H. Schlitt, K. H. Link, W. Bechstein, H.R. Raab, L. Staib, C.T. Germer, T. Liersch, R. Sauer, C. Rödel, M. Ghadimi, W. Hohenberger, Association of plane of total mesorectal excision with prognosis of rectal cancer: secondary analysis of the CAO/ARO/AIO-04 phase 3 randomized clinical trial, JAMA Surg 153 (2018) e181607. https://10.1001/jamasurg.2018.1607.

[6] K. Freischlag, Z. Sun, M.A. Adam, J. Kim, M. Palta, B.G. Czito, J. Migaly, C.R. Mantyh, Association between incomplete neoadjuvant radiotherapy and survival for patients with locally advanced rectal cancer, JAMA Surg 152 (2017) 558–564. https://10.1001/jamasurg.2017.0010.

[7] C.C. Chen, M.L. Wu, K.C. Huang, I.P. Huang, Y.L. Chung, The effects of neoadjuvant treatment on the tumor microenvironment in rectal cancer: implications for immune activation and therapy response, Clin. Colorectal Cancer 19 (2020) e164–e180. https://10.1016/j.clcc.2020.04.002.

[8] S. Saigusa, Y. Toiyama, K. Tanaka, T. Yokoe, Y. Okugawa, H. Fujikawa, K. Matsusita, M. Kawamura, Y. Inoue, C. Miki, M. Kusunoki, Cancer-associated fibroblasts correlate with poor prognosis in rectal cancer after chemoradiotherapy, Int. J. Oncol. 38 (2011) 655–663. https://10.3892/ijo.2011.906.

[9] A. Jarosch, U. Sommer, A. Bogner, C. Reißfelder, J. Weitz, M. Krause, G. Folprecht, G.B. Baretton, D.E. Aust, Neoadjuvant radiochemotherapy decreases the total amount of tumor infiltrating lymphocytes, but increases the number of CD8+/Granzyme B+ (GrzB) cytotoxic T-cells in rectal cancer, OncoImmunology 7 (2018) e1393133. https://10.1080/2162402x.2017.1393133.

[10] Y. Yang, W. Tian, L. Su, P. Li, X. Gong, L. Shi, Q. Zhang, B. Zhao, H. Zhao, Tumor-infiltrating cytotoxic T cells and tumor-associated macrophages correlate with the outcomes of neoadjuvant chemoradiotherapy for locally advanced rectal cancer, Front. Oncol. 11 (2021) 743540. https://10.3389/fonc.2021.743540.

[11] R. Dienstmann, G. Villacampa, A. Sveen, M.J. Mason, D. Niedzwiecki, A. Nesbakken, V. Moreno, R.S. Warren, R.A. Lothe, J. Guinney, Relative contribution of clinicopathological variables, genomic markers, transcriptomic subtyping and microenvironment features for outcome prediction in stage II/III colorectal cancer, Ann. Oncol. 30 (2019) 1622–1629. https://10.1093/annonc/mdz287.

[12] E. Sahai, I. Astsaturov, E. Cukierman, D.G. DeNardo, M. Egeblad, R.M. Evans, D. Fearon, F.R. Greten, S.R. Hingorani, T. Hunter, R.O. Hynes, R.K. Jain, T. Janowitz, C. Jorgensen, A.C. Kimmelman, M.G. Kolonin, R.G. Maki, R.S. Powers, E. Puré, D.C. Ramirez, R. Scherz-Shouval, M.H. Sherman, S. Stewart, T. D. Tlsty, D.A. Tuveson, F.M. Watt, V. Weaver, A.T. Weeraratna, Z. Werb, A framework for advancing our understanding of cancer-associated fibroblasts, Nat. Rev. Cancer 20 (2020) 174–186. https://10.1038/s41568-019-0238-1.

[13] X. Chen, E. Song, Turning foes to friends: targeting cancer-associated fibroblasts, Nat. Rev. Drug Discov. 18 (2019) 99–115. https://10.1038/s41573-018-0004-1.

[14] S. Gonçalves-Ribeiro, R. Sanz-Pamplona, A. Vidal, X. Sanjuan, N. Guillen Díaz-Maroto, A. Soriano, J. Guardiola, N. Albert, M. Martínez-Villacampa, I. López, C. Santos, J. Serra-Musach, R. Salazar, G. Capellà, A. Villanueva, D.G. Molleví, Prediction of pathological response to neoadjuvant treatment in rectal cancer with a two-protein immunohistochemical score derived from stromal gene-profiling, Ann. Oncol. 28 (2017) 2160–2168. https://10.1093/annonc/mdx293.

[15] T.P. Sandberg, M. Stuart, J. Oosting, R. Tollenaar, C.F.M. Sier, W.E. Mesker, Increased expression of cancer-associated fibroblast markers at the invasive front and its association with tumor-stroma ratio in colorectal cancer, BMC Cancer 19 (2019) 284. https://10.1186/s12885-019-5462-2.

[16] J. Tommelein, E. De Vlieghere, L. Verset, E. Melsens, J. Leenders, B. Descamps, A. Debucquoy, C. Vanhove, P. Pauwels, C.P. Gespach, A. Vral, A. De Boeck, K. Haustermans, P. de Tullio, W. Ceelen, P. Demetter, T. Boterberg, M. Bracke, O. De Wever, Radiotherapy-activated cancer-associated fibroblasts promote tumor progression through paracrine IGF1R activation, Cancer Res. 78 (2018) 659–670. https://10.1158/0008-5472.Can-17-0524.

[17] T. Aizawa, H. Karasawa, R. Funayama, M. Shirota, T. Suzuki, S. Maeda, H. Suzuki, A. Yamamura, T. Naitoh, K. Nakayama, M. Unno, Cancer-associated fibroblasts secrete Wnt2 to promote cancer progression in colorectal cancer, Cancer Med. 8 (2019) 6370–6382. https://10.1002/cam4.2523.

[18] Y. Zhang, S. Wang, Q. Lai, Y. Fang, C. Wu, Y. Liu, Q. Li, X. Wang, C. Gu, J. Chen, J. Cai, A. Li, S. Liu, Cancer-associated fibroblasts-derived exosomal miR-17-5p promotes colorectal cancer aggressive phenotype by initiating a RUNX3/MYC/TGF-β1 positive feedback loop, Cancer Lett. 491 (2020) 22–35. https://10.1016/j.canlet.2020.07.023.

[19] Y. Hu, J. Gaedcke, G. Emons, T. Beissbarth, M. Grade, P. Jo, M. Yeager, S.J. Chanock, H. Wolff, J. Camps, B.M. Ghadimi, T. Ried, Colorectal cancer susceptibility loci as predictive markers of rectal cancer prognosis after surgery, Genes Chromosomes Cancer 57 (2018) 140–149. https://10.1002/gcc.22512.

[20] M.E. Ritchie, B. Phipson, D. Wu, Y. Hu, C.W. Law, W. Shi, G.K. Smyth, Limma powers differential expression analyses for RNA-sequencing and microarray studies, Nucleic Acids Res. 43 (2015) e47. https://10.1093/nar/gkv007.

[21] J. Racle, K. de Jonge, P. Baumgaertner, D.E. Speiser, D. Gfeller, Simultaneous enumeration of cancer and immune cell types from bulk tumor gene expression data, Elife 6 (2017). https://10.7554/eLife.26476.

[22] K. Yoshihara, M. Shahmoradgoli, E. Martínez, R. Vegesna, H. Kim, W. Torres-Garcia, V. Treviño, H. Shen, P.W. Laird, D.A. Levine, S.L. Carter, G. Getz, K. Stemke-Hale, G.B. Mills, R.G. Verhaak, Inferring tumour purity and stromal and immune cell admixture from expression data, Nat. Commun. 4 (2013) 2612. https://10.1038/ncomms3612.

[23] A. Subramanian, P. Tamayo, V.K. Mootha, S. Mukherjee, B.L. Ebert, M.A. Gillette, A. Paulovich, S.L. Pomeroy, T.R. Golub, E.S. Lander, J.P. Mesirov, Gene set enrichment analysis: a knowledge-based approach for interpreting genome-wide expression profiles, Proc. Natl. Acad. Sci. U. S. A. 102 (2005) 15545–15550. https://10.1073/pnas.0506580102.

[24] S. Hänzelmann, R. Castelo, J. Guinney, GSVA: gene set variation analysis for microarray and RNA-seq data, BMC Bioinf. 14 (2013) 7. https://10.1186/1471-2105-14-7.

[25] T. Li, J. Fan, B. Wang, N. Traugh, Q. Chen, J.S. Liu, B. Li, X.S. Liu, TIMER: a web server for comprehensive analysis of tumor-infiltrating immune cells, Cancer Res. 77 (2017) e108–e110. https://10.1158/0008-5472.Can-17-0307.

[26] A.M. Newman, C.B. Steen, C.L. Liu, A.J. Gentles, A.A. Chaudhuri, F. Scherer, M.S. Khodadoust, M.S. Esfahani, B.A. Luca, D. Steiner, M. Diehn, A.A. Alizadeh, Determining cell type abundance and expression from bulk tissues with digital cytometry, Nat. Biotechnol. 37 (2019) 773–782. https://10.1038/s41587-019-0114-2.

[27] Y. Lin, J. Xu, H. Lan, Tumor-associated macrophages in tumor metastasis: biological roles and clinical therapeutic applications, J. Hematol. Oncol. 12 (2019) 76. https://10.1186/s13045-019-0760-3.

[28] A.J. Boutilier, S.F. Elsawa, Macrophage polarization states in the tumor microenvironment, Int. J. Mol. Sci. 22 (2021). https://10.3390/ijms22136995.

[29] R. Glynne-Jones, R. Hughes, Critical appraisal of the 'wait and see' approach in rectal cancer for clinical complete responders after chemoradiation, Br. J. Surg. 99 (2012) 897–909. https://10.1002/bjs.8732.

[30] E. Al-Sukhni, K. Attwood, D.M. Mattson, E. Gabriel, S.J. Nurkin, Predictors of pathologic complete response following neoadjuvant chemoradiotherapy for rectal cancer, Ann. Surg Oncol. 23 (2016) 1177–1186. https://10.1245/s10434-015-5017-y.

[31] P.M. Polanco, A.A. Mokdad, H. Zhu, M.A. Choti, S. Huerta, Association of adjuvant chemotherapy with overall survival in patients with rectal cancer and pathologic complete response following neoadjuvant chemotherapy and resection, JAMA Oncol. 4 (2018) 938–943. https://10.1001/jamaoncol.2018.0231.

[32] C. Song, J.H. Chung, S.B. Kang, D.W. Kim, H.K. Oh, H.S. Lee, J.W. Kim, K.W. Lee, J.H. Kim, J.S. Kim, Impact of tumor regression grade as a major prognostic factor in locally advanced rectal cancer after neoadjuvant chemoradiotherapy: a proposal for a modified staging system, Cancers 10 (2018). https://10.3390/cancers10090319.

[33] H. Kobayashi, A. Enomoto, S.L. Woods, A.D. Burt, M. Takahashi, D.L. Worthley, Cancer-associated fibroblasts in gastrointestinal cancer, Nat. Rev. Gastroenterol. Hepatol. 16 (2019) 282–295. https://10.1038/s41575-019-0115-0.

[34] J.L. Hu, W. Wang, X.L. Lan, Z.C. Zeng, Y.S. Liang, Y.R. Yan, F.Y. Song, F.F. Wang, X.H. Zhu, W.J. Liao, W.T. Liao, Y.Q. Ding, L. Liang, CAFs secreted exosomes promote metastasis and chemotherapy resistance by enhancing cell stemness and epithelial-mesenchymal transition in colorectal cancer, Mol. Cancer 18 (2019) 91. https://10.1186/s12943-019-1019-x.

[35] F. Lotti, A.M. Jarrar, R.K. Pai, M. Hitomi, J. Lathia, A. Mace, G.A. Gantt Jr., K. Sukhdeo, J. DeVecchio, A. Vasanji, P. Leahy, A.B. Hjelmeland, M.F. Kalady, J. N. Rich, Chemotherapy activates cancer-associated fibroblasts to maintain colorectal cancer-initiating cells by IL-17A, J. Exp. Med. 210 (2013) 2851–2872. https://10.1084/jem.20131195.

[36] X. Chen, Y. Liu, Q. Zhang, B. Liu, Y. Cheng, Y. Zhang, Y. Sun, J. Liu, Exosomal miR-590-3p derived from cancer-associated fibroblasts confers radioresistance in colorectal cancer, Mol. Ther. Nucleic Acids 24 (2021) 113–126. https://10.1016/j.omtn.2020.11.003.

[37] L. Liu, Z. Zhang, L. Zhou, L. Hu, C. Yin, D. Qing, S. Huang, X. Cai, Y. Chen, Cancer associated fibroblasts-derived exosomes contribute to radioresistance through promoting colorectal cancer stem cells phenotype, Exp. Cell Res. 391 (2020) 111956. https://10.1016/j.yexcr.2020.111956.

[38] J.D. Solano-Iturri, M. Beitia, P. Errarte, J. Calvete-Candenas, M.C. Etxezarraga, A. Loizate, E. Echevarria, I. Badiola, G. Larrinaga, Altered expression of fibroblast activation protein-α (FAP) in colorectal adenoma-carcinoma sequence and in lymph node and liver metastases, Aging 12 (2020) 10337–10358. https://10.18632/aging.103261.

[39] Z. Rong, Z. Luo, Z. Fu, P. Zhang, T. Li, J. Zhang, Z. Zhu, Z. Yu, Q. Li, Z. Qiu, C. Huang, The novel circSLC6A6/miR-1265/C2CD4A axis promotes colorectal cancer growth by suppressing p53 signaling pathway, J. Exp. Clin. Cancer Res. 40 (2021) 324. https://10.1186/s13046-021-02126-y.

[40] B.G. Jang, H.S. Kim, J.M. Bae, W.H. Kim, H.U. Kim, G.H. Kang, SMOC2, an intestinal stem cell marker, is an independent prognostic marker associated with better survival in colorectal cancers, Sci. Rep. 10 (2020) 14591. https://10.1038/s41598-020-71643-1.

[41] A. Shvab, G. Haase, A. Ben-Shmuel, N. Gavert, T. Brabletz, S. Dedhar, Ben-Ze'ev A, Induction of the intestinal stem cell signature gene SMOC-2 is required for L1-mediated colon cancer progression, Oncogene 35 (2016) 549–557. https://10.1038/onc.2015.127.

[42] D. Unterleuthner, P. Neuhold, K. Schwarz, L. Janker, B. Neuditschko, H. Nivarthi, I. Crncec, N. Kramer, C. Unger, M. Hengstschläger, R. Eferl, R. Moriggl, W. Sommergruber, C. Gerner, H. Dolznig, Cancer-associated fibroblast-derived WNT2 increases tumor angiogenesis in colon cancer, Angiogenesis 23 (2020) 159–177. https://10.1007/s10456-019-09688-8.

[43] R. Wang, Y. Sun, W. Yu, Y. Yan, M. Qiao, R. Jiang, W. Guan, L. Wang, Downregulation of miRNA-214 in cancer-associated fibroblasts contributes to migration and invasion of gastric cancer cells through targeting FGF9 and inducing EMT, J. Exp. Clin. Cancer Res. 38 (2019) 20. https://10.1186/s13046-018-0995-9.

[44] Y. Zhang, J. Zhao, M. Ding, Y. Su, D. Cui, C. Jiang, S. Zhao, G. Jia, X. Wang, Y. Ruan, Y. Jing, S. Xia, B. Han, Loss of exosomal miR-146a-5p from cancer-associated fibroblasts after androgen deprivation therapy contributes to prostate cancer metastasis, J. Exp. Clin. Cancer Res. 39 (2020) 282. https://10.1186/s13046-020-01761-1.

[45] Y.Y. Li, Y.W. Tao, S. Gao, P. Li, J.M. Zheng, S.E. Zhang, J. Liang, Y. Zhang, Cancer-associated fibroblasts contribute to oral cancer cells proliferation and metastasis via exosome-mediated paracrine miR-34a-5p, EBioMedicine 36 (2018) 209–220. https://10.1016/j.ebiom.2018.09.006.

[46] Y. Xu, R. Kuai, Y.M. Chu, L. Zhou, H.Q. Zhang, J. Li, Hypoxia facilitates the proliferation of colorectal cancer cells by inducing cancer-associated fibroblast-derived IL6, Neoplasma 68 (2021) 1015–1022. https://10.4149/neo_2021_210308N296.

[47] K. Yang, J. Zhang, C. Bao, Exosomal circEIF3K from cancer-associated fibroblast promotes colorectal cancer (CRC) progression via miR-214/PD-L1 axis, BMC Cancer 21 (2021) 933. https://10.1186/s12885-021-08669-9.

[48] R. Lappano, M. Talia, F. Cirillo, D.C. Rigiracciolo, D. Scordamaglia, R. Guzzi, A.M. Miglietta, E.M. De Francesco, A. Belfiore, A.H. Sims, M. Maggiolini, The IL1β-IL1R signaling is involved in the stimulatory effects triggered by hypoxia in breast cancer cells and cancer-associated fibroblasts (CAFs), J. Exp. Clin. Cancer Res. 39 (2020) 153. https://10.1186/s13046-020-01667-y.

[49] Y. Pan, Y. Yu, X. Wang, T. Zhang, Tumor-associated macrophages in tumor immunity, Front. Immunol. 11 (2020) 583084. https://10.3389/fimmu.2020.583084.

[50] R. Zhang, F. Qi, F. Zhao, G. Li, S. Shao, X. Zhang, L. Yuan, Y. Feng, Cancer-associated fibroblasts enhance tumor-associated macrophages enrichment and suppress NK cells function in colorectal cancer, Cell Death Dis. 10 (2019) 273. https://10.1038/s41419-019-1435-2.

[51] A. Zhang, Y. Qian, Z. Ye, H. Chen, H. Xie, L. Zhou, Y. Shen, S. Zheng, Cancer-associated fibroblasts promote M2 polarization of macrophages in pancreatic ductal adenocarcinoma, Cancer Med. 6 (2017) 463–470. https://10.1002/cam4.993.

[52] G. Comito, E. Giannoni, C.P. Segura, P. Barcellos-de-Souza, M.R. Raspollini, G. Baroni, M. Lanciotti, S. Serni, P. Chiarugi, Cancer-associated fibroblasts and M2-polarized macrophages synergize during prostate carcinoma progression, Oncogene 33 (2014) 2423–2431. https://10.1038/onc.2013.191.

[53] M. Balsamo, F. Scordamaglia, G. Pietra, C. Manzini, C. Cantoni, M. Boitano, P. Queirolo, W. Vermi, F. Facchetti, A. Moretta, L. Moretta, M.C. Mingari, M. Vitale, Melanoma-associated fibroblasts modulate NK cell phenotype and antitumor cytotoxicity, Proc. Natl. Acad. Sci. U.S.A. 106 (2009) 20847–20852. https://10.1073/pnas.0906481106.

[54] T. Kinoshita, G. Ishii, N. Hiraoka, S. Hirayama, C. Yamauchi, K. Aokage, T. Hishida, J. Yoshida, K. Nagai, A. Ochiai, Forkhead box P3 regulatory T cells coexisting with cancer associated fibroblasts are correlated with a poor outcome in lung adenocarcinoma, Cancer Sci. 104 (2013) 409–415. https://10.1111/cas.12099.